https://doi.org/10.5194/egusphere-2024-2149
Preprint. Discussion started: 15 August 2024

OF-CEAS laser spectroscopy to measure water isotopes in dry environments: example of application in Antarctica

Thomas Lauwers[1], Elise Fourré[1], Olivier Jossoud[1], Daniele Romanini[3], Frédéric Prié[1], Giordano Nitti[1], Mathieu Casado[1], Kévin Jaulin[2], Markus Miltner [2,3], Morgane Farradèche[1], Valérie Masson – Delmotte[1], Amaëlle Landais[1]

[1]Laboratoire des Sciences du Climat et de l'Environnement – IPSL, UMR 8212, CEA-CNRS-UVSQ, Paris-Saclay University, Gif-sur-Yvette, France
[2]AP2E, 110 av. Galilée, 13290 Aix en Provence, France
[3]Université Grenoble Alpes, CNRS, LIPhy UMR 5588, 38041 Grenoble, France

Correspondence to: Thomas Lauwers (thomas.lauwers@lsce.ipsl.fr)

Abstract. Water vapour isotopes are important tools to better understand processes governing the atmospheric hydrological cycle. Their measurement in polar regions is crucial to improve the interpretation of water isotopic records in ice cores. *In situ* water vapour isotopic monitoring is however an important challenge, especially in dry places of the East Antarctic plateau where water mixing ratio can be as low as 10 ppmv. We present in this article new commercial laser spectrometers based on the optical feedback – cavity enhanced absorption spectroscopy (OF-CEAS) technique, adapted for water vapour isotopic measurement in dry regions. We characterize a first instrument adapted for Antarctic coastal monitoring with an optical cavity finesse of 64,000 (ringdown time of 54 µs), installed at Dumont d'Urville station during the summer campaign 2022-2023, and a second instrument with a high finesse of 116,000 (98 µs ringdown), to be deployed inland East Antarctica. The high finesse instrument demonstrates a stability up to two days of acquisition, with a limit of detection down to 10 ppmv humidity for δD and 100 ppmv for δ^{18}O.

Introduction

Stable water vapour isotopes monitoring (mainly $H_2{}^{16}O$, $H_2{}^{18}O$ and $HD^{16}O$) in the atmosphere helps to understand a number of processes governing the atmospheric water cycle (Galewsky et al., 2016), such as phase change (Merlivat and Nief, 1967; Benetti et al., 2018; Hughes et al., 2021), transport (Bonne et al., 2020), or mixing of air masses. Until the 1990s, the first techniques for water vapour isotopic composition monitoring relied on sampling with cryogenic traps and subsequent mass spectrometry measurements (Angert et al., 2008), but it was time consuming and not easy to implement in a broad variety of environments.

Today, laser spectrometers are a solution for such *in situ* continuous measurements (Gupta et al., 2009; Landais et al., 2024). Isotope analysers use near infrared laser diodes and most of them are based either on the cavity ring-down spectroscopy (CRDS) technique or cavity enhanced absorption spectroscopy technique (CEAS). The CRDS method is commonly implemented by Picarro company, and gives a high stability through the measurement of the photon lifetime inside the optical cavity instead of the direct absorbed light. Those instruments are robust and adapted for field measurement. A broad number of studies used stable water vapour isotopes to document the evolution of the atmospheric water cycle over synoptic events (e.g. cold fronts, cyclones) (Aemisegger et al., 2015; Bhattacharya et al., 2022; Tremoy et al., 2014) or to understand processes within the water cycle (e.g. evaporation over the ocean) (Benetti et al., 2015). Instruments are no longer only installed in observatory stations but can be found on board of boats (Thurnherr et al., 2020) or aircrafts (Henze et al., 2022). An increasing number of studies is also now devoted to the study of the atmospheric water cycle in the polar regions with the objective to document either the atmospheric dynamics (e.g. atmospheric rivers, synoptic events, influence of katabatic winds) (Bonne et al., 2014; Bréant et al., 2019; Kopec et al., 2014; Leroy-Dos Santos et al., 2021, 2023) or the exchange between snow and water vapour at the surface of the ice sheets (Casado et al., 2016; Ritter et al., 2016; Wahl et al., 2021). Those last studies are

https://doi.org/10.5194/egusphere-2024-2149
Preprint. Discussion started: 15 August 2024

essential to interpret the water isotopic records in ice core which are not only driven by temperature and condensation along the transportation of water vapour from the evaporative to the polar regions but also influenced by equilibrium / diffusive processes in the upper snow (Dietrich et al., 2023). However, CRDS struggle to properly measure the isotopic composition in very dry conditions (water mixing ratio below 500 ppm) (Leroy-Dos Santos et al., 2021), that can be encountered in polar regions or in altitude, so that isotopic processes in key regions like inland Antarctica can only be documented during summer (Casado et al., 2016; Ritter et al., 2016).

To overcome this limitation, we present in this article instruments based on an alternative technique called OF-CEAS, which combines the CEAS method and an optical feedback (OF) from a V-shaped cavity, allowing to narrow down the laser emission frequency by locking it to the cavity resonances. This provides efficient cavity injection and low noise cavity output from all resonances across the laser scan. The maxima of these resonances provide directly the cavity enhanced spectrum, converted to an absolute absorption scale using a ring-down produced by shutting off the laser at the last resonance in the laser scan (Romanini et al., 2014). This technique was first implemented for water vapour isotope analysis with a laboratory prototype (Landsberg et al., 2014) but never successfully deployed in the field, with stable working conditions. We present in this paper the performance obtained with new commercial OF-CEAS analysers, developed in collaboration with the AP2E company (ProCeas®) and specifically designed to measure water vapour isotopes in a very dry environment. After a brief description of the laser spectrometer and the auxiliary calibration instrument, we present the analyser stability, its water mixing ratio response, and its accuracy and precision in dry conditions. We finally discuss the instrumental performance compared to already available commercial instruments manufactured by Picarro, and propose a calibration procedure adapted for continuous water vapour isotopes monitoring using OF-CEAS instruments.

1 Instrumental development

1.1 OF – CEAS spectrometer

Water isotopes OF-CEAS spectrometers use a distributed feedback laser source centred around 1389 nm to target the three water absorption lines of HDO (7200.3023 cm^{-1}), $H_2{}^{16}O$ (7200.1335 cm^{-1}) and $H_2{}^{18}O$ (7199.9614 cm^{-1}). As shown in the spectrum on Figure 1, the absorption lines of interest can be affected by the presence of methane and strong absorption lines of water located outside the spectral window.

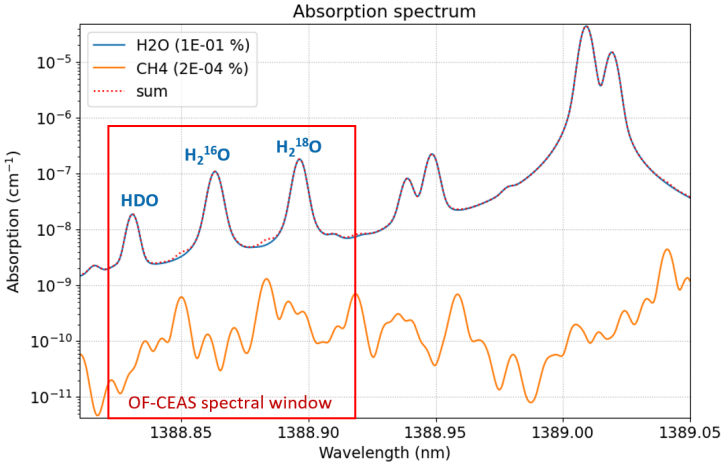

Figure 1 : Absorption spectrum of the three target isotopologues HDO, $H_2{}^{16}O$ and $H_2{}^{18}O$ retrieved from HITRAN database. The total absorption spectrum is plotted with the red dotted line, considering 1% of water vapour (blue line) and 2 ppm of methane (orange line). The red rectangle indicates the OF-CEAS spectral window by current tuning on a 1389 nm distributed feedback laser diode.

https://doi.org/10.5194/egusphere-2024-2149
Preprint. Discussion started: 15 August 2024

The centring of the spectral window is performed by tuning the temperature of the laser source whereas the fast wavelength scan is performed by tuning the laser current. With a V-shaped cavity length of about 40 cm resulting in a free spectral range (FSR) of 188 MHz, the wavelength range of interest contains 80 resonance modes, as shown in Figure 2 (blue dots). The shown spectrum was obtained after a long injection of dry Nitrogen, resulting in a minimal absolute humidity of 3 ppm. The residuals (difference between the fitted and acquired spectrum) are shown by the orange line. To perform the spectral fitting, the physical spectroscopic values are first retrieved from the Hitran database (mainly the relative position of the peaks, intensities, Gaussian and Lorentzian width), and used as initial parameters. Then, the parameters are empirically tuned to obtain the smallest and flattest residuals. For example, a symmetric shape of the residuals around the peaks like a M-shape or a W-shape would indicate an incorrect width, while an asymmetric shape would indicate a non-optimized peak position. The resulting residuals after optimization show a uniform repartition, with a peak-to-peak value of 1.2×10^{-10} cm^{-1}, as shown in Figure 2.

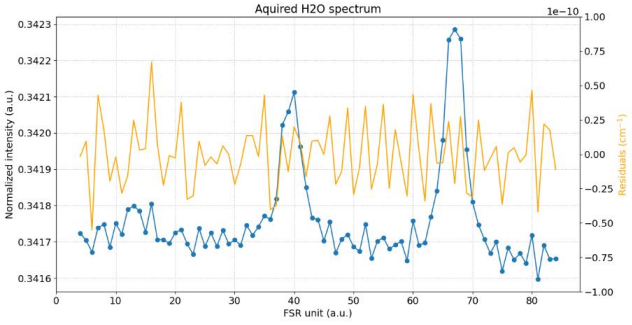

Figure 2 : Measured spectrum of the OF-CEAS analyser (blue dots) after a long drying using a N_2 gas cylinder, resulting in a minimal water concentration of 3 ppm. The residuals after fitting are expressed in cm^{-1} (yellow line) and obtained from a 600 ms wavelength scan and a fit calculation time of less than 52 ms,

For a ring-down of 98 µs, and an acquisition of 80 modes, the wavelength scan is performed in 600 ms to enable at the same time a correct signal to noise ratio and an interesting time resolution for the analysis of transient water vapour phenomena. In order to keep a fast, real time data acquisition, the fitting algorithm is tuned so that most parameters are fixed. The typical calculation time is of 52 ms in steady operation, which is shorter than the wavelength scan time.

1.2 Low humidity level generator

For continuous water vapour isotopic measurement, the performance of the analyser must be characterized in terms of stability over time (Allan deviation) and water mixing ratio (hereafter called humidity) dependency of the isotopic measurements (Weng et al., 2020). Additionally, during in-situ measurements, a periodic calibration at one specific humidity is required for drift correction, as the optical signal can be affected by several time-dependent factors, such as temperature or mechanical perturbations.

The characterization of the instrument is performed with a custom laboratory *low humidity level generator* (LHLG) (Leroy-Dos Santos et al., 2021), which enables the generation of a steady water vapour flux with a known and stable isotopic value. A water droplet is generated at the tip of a needle inside an evaporation chamber, flushed by a controlled dry air flux. By controlling both the water and air fluxes, it is possible to precisely control the humidity content of the generated moist air, while the isotopic value is defined by the water sample (Kerstel, 2021) .

The calibration results shown in this paper are carried out with a new version of the LHLG. An updated architecture gives an easy access to the various elements of the instrument (including electronics), while remaining compact and adapted for field operation. Among its new features, the evaporation chambers are now equipped with cartridge heaters to reach higher humidity levels. With a regulated temperature of 60°C inside the evaporation chambers, a stable humidity above 10,000 ppm can be

https://doi.org/10.5194/egusphere-2024-2149
Preprint. Discussion started: 15 August 2024

reached, whereas the older version was limited to a maximal humidity of ~ 2,000 ppm. A sequencer was also implemented in the LHLG software, enabling long calibrations with automatic syringe refill cycles. This permits to assess the spectrometer stability on longer timescales, with several days of stable standard injection.

2 Performance of the instruments

We present in this section the characterisation results of two OF-CEAS instruments manufactured by AP2E company. The first analyser, which we will refer to as "high-humidity analyser" (serial number #1087) has a cavity ring-down time of 54 µs and was installed and characterised at the Dumont d'Urville station (66°40′ S, 140°01′ E) during the austral summer seasons 2022 – 2023 and 2023 – 2024. The second analyser, featuring higher reflectivity mirrors, has a ring-down time of 98 µs and was entirely characterised in the laboratory. This analyser will be referred to as "low humidity analyser" (serial number #1169).

2.1 Time stability

To quantitively assess the mid- and long-term stability of the OF-CEAS instruments, we used the LHLG to perform Allan deviations measurements (from few hours to one week) and drift measurements over one year with regular automatic calibrations.

2.1.1 Allan deviation study

The OF-CEAS stability is assessed at 500 ppm and 100 ppm, which correspond to a LHLG infused water rate of 0.1125 µL/min and 0.0225 µL/min, respectively. As the LHLG is equipped with 100 µL syringes, a one-week long measurement is performed by generating successive plateaus separated by a gap of ~1-2 hours necessary for the syringe refill and the humidity and isotopic composition stabilisation. Figure 3 shows laboratory measurements on the "low-humidity" analyser of (from top to bottom) the humidity, the $\delta^{18}O$ and the δD at 500 ppm (blue) and 100 ppm (red). For comparison, an additional dataset at 1000 ppm from the "high-humidity" analyser is plotted in green. Very stable plateaus are obtained from the LHLG, reaching a standard deviation of 3.1 ppm at 100 ppm during a one-week sequence.

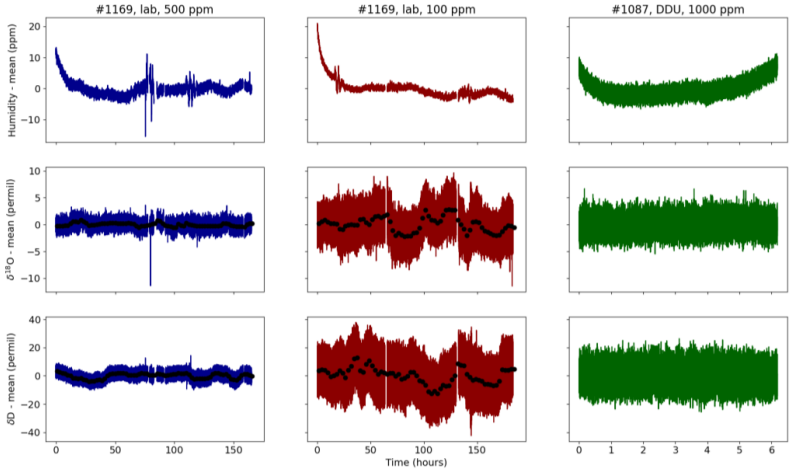

Figure 3 : From top to bottom, measured humidity, δ^{18}O and δD used for the Allan deviation study, referenced to their mean value. The two first columns correspond to one-week calibrations in the lab with the low-humidity analyser at 500 ppm (first column, blue) and at 100 ppm (second column, red). The third column (green) corresponds to the data obtained at 1000 ppm from the high-humidity analyser in the field, over 6 hours. Coloured curves show the raw signal, and the black circles the signal averaged on a 8 000 s window.

https://doi.org/10.5194/egusphere-2024-2149
Preprint. Discussion started: 15 August 2024

To calculate the long-term Allan deviation of the original data containing gaps (blue and red dataset in Figure 3), a secondary dataset is calculated with a time sampling greater than the gap duration, Δt = 8,000s (black points). The long-term Allan deviation (AD) shown in Figure 4 results from merging the AD of the two datasets. We show in blue and red the long-term AD obtained with the low-humidity analyser at 500 ppm and 100 ppm, respectively. The 500 ppm AD is obtained from a sequence of 14 plateaus with a duration of 13 hours each, while the 100 ppm AD is calculated from 3 plateaus with durations of 65 hours each, and the light colour envelope shows the standard deviation associated with the AD of each individual plateau. The use of the second dataset enables to reach a time range spanning from 8,000 s to two days. For comparison, we added in green the AD obtained from a 6-hour sequence performed at 1000 ppm with the high-humidity instrument (ref. #1087).

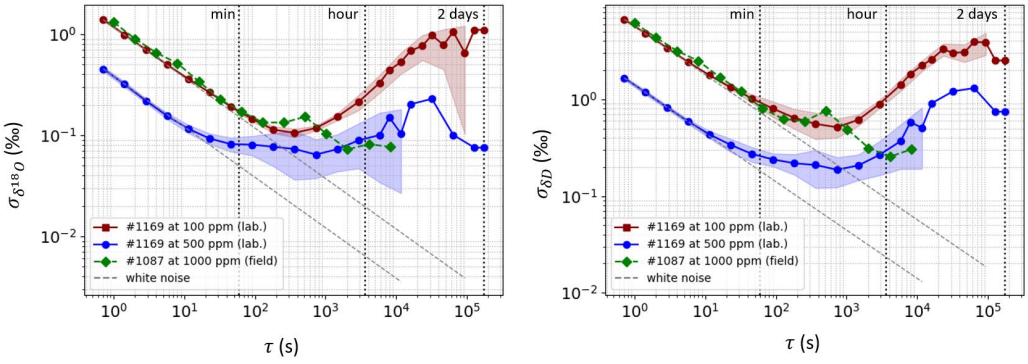

Figure 4 : Allan deviation of $\delta^{18}O$ (left) and δD (right) for a 1000 ppm step performed in the field with the high-humidity analyser (green diamonds, ref #1087) and a 500 ppm sequence (blue circles) and 100 ppm sequence (red squares) performed in the laboratory with the low-humidity analyser (ref. #1169). The grey dashed lines indicate the white noise law $1/\sqrt{t}$. The data retrieved from the high-humidity analyser was archived with a sampling time of 1 s, and of 0.7 s for the low-humidity analyser.

The ADs of the low-humidity analyser follow a white noise decay during several minutes, with a minimal value of 0.1 ‰ (resp. 0.06 ‰) for $\delta^{18}O$ at 100 ppm (resp. 500 ppm) and 0.5 ‰ (resp. 0.2 ‰) for δD at 100 ppm (resp. 500 ppm). A drift is observed after approximately 10 min, which we attribute to parasitic interferences arising along the laser to cavity optical path. After a few hours, we observe that the interference phenomena average out, leading to a stabilisation of the AD over long timespans. After two days, we calculate an AD of 1 ‰ (resp. 0.09 ‰) for $\delta^{18}O$ at 100 ppm (resp. 500 ppm) and of 2.5 ‰ (resp. 0.7 ‰) for δD at 100 ppm (resp. 500 ppm). Finally, the AD of the high-humidity instrument (54 µs ring-down) at 1000 ppm shows a white noise equivalent to the 100 ppm AD obtained from the low-humidity instrument (98 µs ring-down). We also note that no particular drift is observed on the high-humidity instrument in the hourly region because 6 hours is too short to observe mid-term perturbations. This comparison shows that increasing the cavity ring-down time leads to an increase of the signal–to–noise ratio and confirm thus the need for high reflectivity mirrors to target high sensitivities in low-humidity environments.

2.1.2 Long-term stability at Dumont d'Urville station

During in-situ measurements, a periodic calibration is performed to check and eventually correct for instrumental drift on longer time scales, caused by internal instabilities originating from the instrument like parasitic interferences or external perturbations (lab temperature, vibrations, etc). Since this paper presents the first field deployment of an OF-CEAS instrument dedicated to H_2O isotopic analysis, long term drift was a particular concern, requiring a quantitative study. At the Dumont d'Urville (DDU) station, the periodic drift calibration consists in a first step of drying (45 minutes) to remove residual, atmospheric water vapour isotopes, and two successive steps with two standards at a humidity of 1000 ppm (110 minutes in

https://doi.org/10.5194/egusphere-2024-2149
Preprint. Discussion started: 15 August 2024

total). This calibration sequence has been set every 46 hours and is the result of the compromise between frequent calibrations and the time dedicated to atmospheric data acquisition.

We present here the calibration points performed all over the year 2023 – with a gap from mid-June to mid-July due to a breakdown of the LHLG – using two in-house standards calibrated against the IAEA VSMOW/SLAP scale FP5 ($\delta^{18}O$ = - 50.52 ± 0,05 ‰ and δD = - 394.7 ± 0,7 ‰), and AO1 ($\delta^{18}O$ = - 30.6 ± 0,05 ‰ and δD = - 238.3 ± 0,7 ‰). The OF-CEAS calibrations are compared to the values obtained on a L2130-i Picarro instrument (CRDS technology) already running in this station (Leroy-Dos Santos et al., 2023). Each data point in Figure 5 corresponds to the mean value taken over a minimum 5-minute window at the end of the humidity step, with blue circles for the OF-CEAS analyser (AP2E company) and green circles for the CRDS analyser (Picarro company). An additional filtering has been applied to remove the points with a non-stable humidity, i.e. with a humidity value standing outside the 2-σ interval.

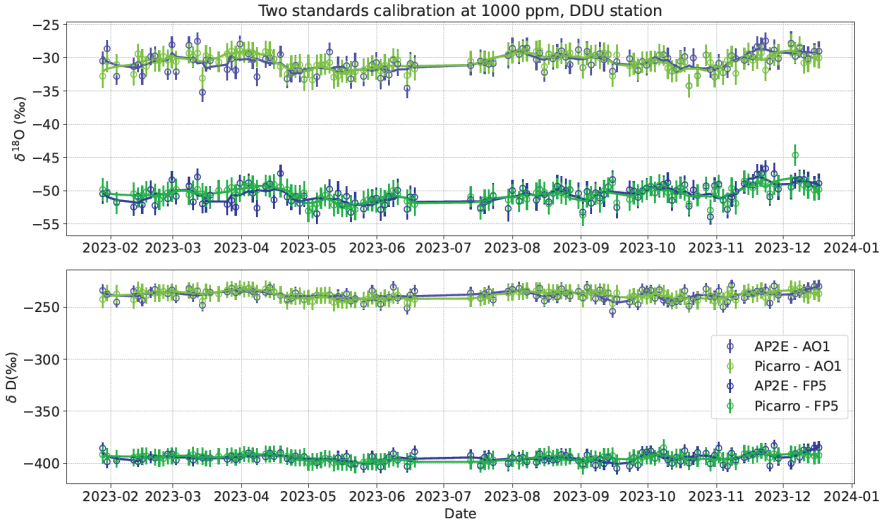

Figure 5 : Drift calibration of the Picarro CRDS and AP2E OF-CEAS laser spectrometers for two in-house isotopic standards named AO1 and FP5. Each point represents the average of the final minimum 5 minutes of 1000 ppm humidity plateaus and the error bars correspond to the associated standard deviation.

The resulting data show no long-term trend on a one-year range neither for the AP2E nor for the Picarro instrument, with a higher dispersion on the OF-CEAS dataset (see Table 1 below). We note also that the analysers calibrations show a correlation on a monthly scale, which could indicate a drift of the calibration instrument. Indeed, important temperature variation have been registered inside the shelter (5°C of maximal amplitude during summer season), which has an impact on the time response of the calibration plateaus and thus the value of the isotopic composition at the end of the plateau. This points out the need for a temperature regulation in the building housing the instruments at DDU and/or inside the evaporation chamber of the calibration instrument.

	OF-CEAS (AP2E)		**CRDS (Picarro)**	
	$\sigma(\delta^{18}O)$	$\sigma(\delta D)$	$\sigma(\delta^{18}O)$	$\sigma(\delta D)$
First standard (AO1)	1.6 ‰	4.9 ‰	1.2 ‰	3.7 ‰
Second standard (FP5)	1.5 ‰	4.5 ‰	1.2 ‰	3.0 ‰

Table 1: Standard deviation of the two standards isotopic calibration performed from January to December 2023 on the OF-CEAS and CRDS analysers.

https://doi.org/10.5194/egusphere-2024-2149
Preprint. Discussion started: 15 August 2024

2.2 Humidity and isotopic composition dependency

We present in this section the characterisation referred in the litterature as the mixing ratio dependency (Weng et al., 2020). Indeed, for a water vapour sample with a given isotopic composition, the measure of the isotopic value can be affected by the humidity level (through different processes, such as spectroscopic effect affecting the fitting procedure, or memory effect). In addition, this behaviour as a function of humidity can differ for different isotopic ranges, especially at low humidity contents (Casado et al., 2016), (Leroy-Dos Santos et al., 2021), (Weng et al., 2020). For this reason, we determined the humidity dependency calibration with two water isotopic standards corresponding to the expected isotopic range in the field. Two calibrated standards (calibrated against the IAEA VSMOW/SLAP scale) are used for the laboratory calibration: the OC4 standard, highly depleted and adapted for measurement on the Antarctic plateau ($\delta^{18}O$ = -53,93 ± 0,05 ‰, δD = -422,7 ± 0,7 ‰) and a lightly depleted standard ROSS7, close to the water vapour isotopic composition of coastal sites ($\delta^{18}O$ = -18,94 ± 0,05 ‰, δD = -146,0 ± 0,7 ‰). Field calibrations are also presented in this section, using the additionnal calibrated standards AO1 and FP5 covering a similar range.

First, the humidity dependency of $\delta^{18}O$ and δD is established taking as a reference the measured value at a given humidity h_{ref}, generally chosen in the range of observed values at the site of interest (Figure 6). A fit of the calibration points gives then the correction function f_{calib}, which verifies the condition $f_{calib}(h_{ref}) = 0$ and is further used for correcting the acquired isotopic data. As the humidity dependency can be different from one standard to another, different strategies can be used to estimate the correction function (Weng et al., 2020). If the target isotopic range is narrow enough or the correction functions are similar from one standard to another, a global fit using the data of several standards in an undifferentiated way can be performed. In the case of divergent correction functions, it is more reliable to make a humidity dependency calibration with two standards, and then define a general, two-dimensional calibration function, defined as the linear interpolation between the two correction functions. Once the calibration points are fitted, for a given humidity h and measured isotopic value δ_{raw}, the data is corrected as follows:

$$\delta_{corr} = \delta_{raw} - f_{calib}(h, \delta_{raw})$$

We show in Figure 6 the characterisation obtained with the analyser adapted for low humidity (left column) and for high humidity environments (right column). The calibration of the low-humidity analyser was performed in the lab, and repeated several times within a 3-months period, with the very depleted standard OC4 (blue circles) and the lightly depleted standard ROSS7 (red squares) and a reference humidity fixed at 500 ppm. For the low humidity analyser shades of blue and red indicate the various series of measurement acquired between March (light colour) and May 2023 (dark colour). The high-humidity analyser calibration was performed at Dumont d'Urville station during a 48 hours-long sequence, using the highly depleted standard FP5 (blue triangles) and the lightly depleted standard AO1 (red diamonds), in December 2022 (light colour) and December 2023 (dark colour). The vertical, red dotted line indicates that more than 99% of the absolute humidity at DDU stay above this threshold, i.e. in the linear region. A reference humidity of 1000 ppm was chosen here, as it is situated closer to the usual humidity values measured on the Antarctic coast. For the field calibration, a first humidity sequence was performed in the low humidity region (50-1,500 ppm) and a second run for the high humidity region (2,000-6,000 ppm), using a heated evaporation chamber (60°C).

Two distinct regimes can be highlighted from the humidity dependency (Figure 6). Below 500 ppm, we observe a divergence of the isotopic value (here assimilated to a 1/x function) with distinct trends for the highly depleted (blue) and lightly depleted (red) standards. Above 500 ppm, the two curves merge and a linear dependency for $\delta^{18}O$ and δD is observed on both instruments. For the high-humidity analyser, we observe a good superposition for the humidity response of the two standards AO1 and FP5 from 6,000 to 500 ppm, corresponding to more than 99% of the humidity values usually recorded at DDU station. The measured slopes of the humidity response in the 500 – 6000 ppm region are reported in Table 2.

https://doi.org/10.5194/egusphere-2024-2149
Preprint. Discussion started: 15 August 2024

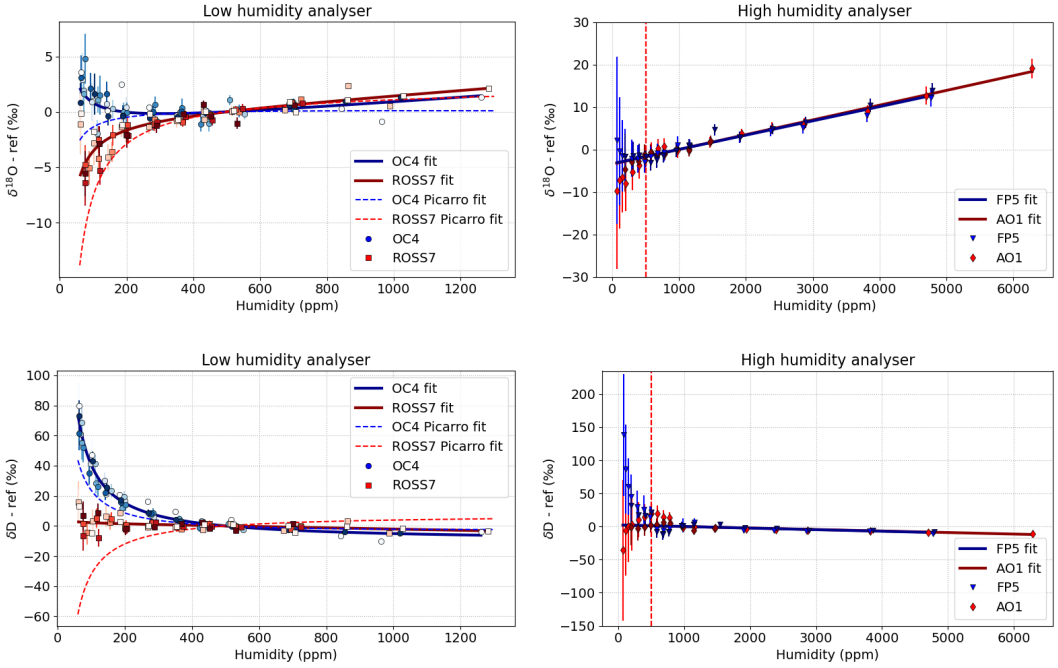

Figure 6 : Humidity dependency calibration of the low-humidity OF-CEAS analyser from 50 to 1300 ppm for $\delta^{18}O$ (top left) and δD (bottom left) and of the high-humidity analyser from 50 to 6500 ppm for $\delta^{18}O$ (top right) and δD (bottom right). Shades of blue and red indicate various calibration sequences. Additional dashed curves correspond to the typical humidity dependency of a Picarro instrument measured in the lab, for comparison. The vertical dashed line in the left panels corresponds to the humidity above which 99% of the humidity signal at DDU is observed.

The positive slope on the $\delta^{18}O$ calibration curve is explained by the presence of a strong absorption line of water situated around 1389 nm (as shown in Figure 1), creating a shift of the baseline and a bias on the fit, while for δD this creates a negative slope. As the HDO absorption line is situated further away than the large water absorption peak, the slope has a smaller amplitude. Below 500 ppm, we observe a larger noise on the high-humidity analyser (#1087) installed at DDU, which features lower reflectivity mirrors (ring-down of 54 µs) than the low-humidity analyser (#1169, ring-down of 98 µs) characterized in the laboratory.

	Slope from high-humidity #1087 analyser (‰ / 1000 ppm)		
	Lightly depleted	**Highly depleted**	**Mean**
$\delta^{18}O$	3.1	3.0	3.1
δD	-2.7	-2.2	-2.5

Table 2: Slope of the humidity dependency calibration on the high humidity spectrometer, in the 500 - 6000 ppm region, expressed in ‰/1000 ppm.

The characterisation performed on both analysers highlights that no significant drift is observed between the humidity dependency calibrations, over a one-year timespan, and that a linear, global correction function can be applied above 500 ppm. Below 500 ppm we need to consider the divergence between the two standards by using a two-dimensional correction function defined as the linear interpolation between the lightly depleted and the highly depleted standard correction function.

https://doi.org/10.5194/egusphere-2024-2149
Preprint. Discussion started: 15 August 2024

2.3 Instrument accuracy against the VSMOW-SLAP scale

We demonstrated the stability of the instrument for short to mid-term time spans with the Allan deviation and for longer time period with repeated humidity calibrations during one year. After having estimated the humidity dependency correction of the OF-CEAS analyser, we present in this section the instrument accuracy against the VSMOW-SLAP scale, using a linear calibration from two standards, following the NIST recommendation (Reference Material 8535). An additional standard situated inside the isotopic range is used to quantify the precision and accuracy of the measure.

Figure 7 shows the relation between the measured isotopic value and the true value for the two standards OC4 and ROSS7, and the measurements of an additional standard TD3 for various humidity steps ranging in the divergence area, from 67 to 698 ppm. From the linear relationship obtained with OC4 and ROSS7 (black dashed line), the expected value for TD3 (red triangle) shows an accuracy of 0.7 ‰ for $\delta^{18}O$ and 1.7 ‰ for δD, compared to the independent VSMOW-calibrated value, $\delta^{18}O$ = - 40.19 ± 0,05 ‰ and δD = - 313.6 ± 0,7 ‰ and a precision in this humidity range of 0.4 ‰ for $\delta^{18}O$ and 3.6 ‰ for δD.

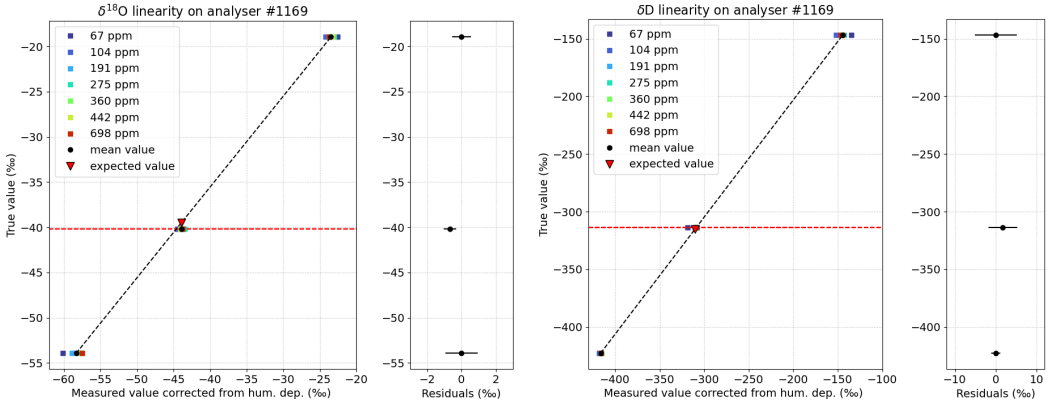

Figure 7: Correspondence between the true isotopic value and the measured, corrected value of $\delta^{18}O$ and δD for 7 humidity steps ranging from 67 to 698 ppm with three VSMOW-SLAP calibrated standards OC4, TD3 and ROSS7 (coloured squares), with the corresponding average values calculated across the humidity range (black circles). The linear calibration slope (black dashed line) results from the average value of the OC4 and ROSS7 standards only, while the TD3 standard (true value indicated with the red dashed line) is used to quantify the instrument accuracy and precision. The red triangle indicates the expected value of the TD3 standard using the calibration slope.

3 Discussion

3.1 Expected performance for in situ water vapour isotope measurement in the frame of the AWACA project using OF-CEAS technology

In addition to the already installed analyser at DDU station, several OF-CEAS analysers will be deployed during the austral summer 2024-2025 in remote sites, from the Antarctic coast (DDU station) to the plateau above 3200 m (Concordia station). The three chosen remote sites, named D17, D47 and D85, as well as Concordia station (DC) are shown in Figure 8. The instrumental deployment will be achieved in the framework of AWACA (Atmospheric WAter Cycle over Antarctica) project, whose objective is to provide a comprehension of the past, present and future atmospheric branch of the Antarctic water cycle. To give a quantitative overview of the expected performances for this deployment, we calculated for each site the proportion of days per year with average humidity below 500, 100 and 10 ppm (retrieved from automatic weather stations in 2018 for D85 and in 2020 for the other sites), see Figure 8, left. For each humidity value, a long-term AD measurement is performed on the low-humidity analyser using the method presented in part 2.2., and its value after 24 hours is plotted. At 500 ppm and 100 ppm, the LHLG enables repeated injections of ROSS7 standard with the procedure described in section 2.1.1. An

https://doi.org/10.5194/egusphere-2024-2149
Preprint. Discussion started: 15 August 2024

additional step at 10 ppm is performed and corresponds to residual water obtained by a pure drying using the LHLG without any water sample injection. We plotted in Figure 8 left, in red (resp. dark red) the AD of $\delta^{18}O$ (resp. dD).

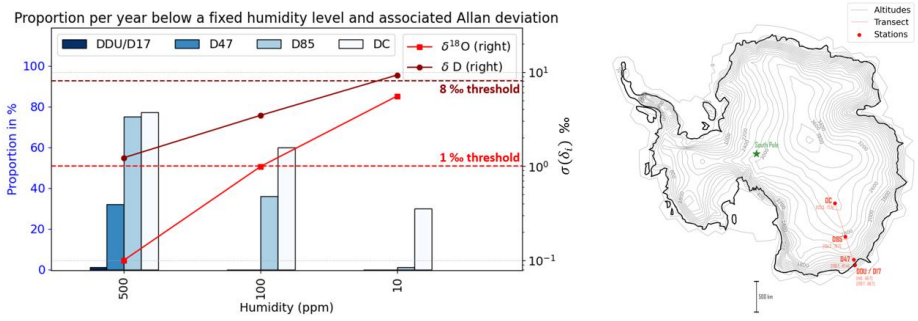

Figure 8 : On the left, histogram representing the year fraction (expressed in %) below a fixed humidity content for 4 sites situated along the transect. For each humidity, we plotted the associated Allan deviation σ(δi) after 24 hours for δ18O and δD. The dotted horizontal lines represent the δ18O and δD upper thresholds for diurnal cycle tracking, in red and dark red, respectively (see discussion in the text). On the right, map with the location of the 4 instrumented sites for the AWACA deployment.

As typical diurnal cycles of the water vapour isotope are of the order of 10 ‰ for $\delta^{18}O$ (resp. ~ 80 ‰ for δD) at Dumont d'Urville and Dome C - Concordia (Casado et al., 2016), (Bréant, 2019), we suggest a noise threshold of 1 ‰ for $\delta^{18}O$ and of 8 ‰ for δD, above which we consider that no interpretation of the isotopic signal at the diurnal scale can be confidently made. This threshold value is indicated on the figure by the horizontal dotted line. We observe on average a larger noise for δD, explained by the smaller absorption intensity of the HDO line compared to the $H_2{}^{18}O$ line. However, while the $\delta^{18}O$ deviation crosses the threshold noise at around 100 ppm, the δD deviation stays below the 8 ‰ threshold, until approximately 10 ppm. We can conclude from this characterization that we should preferably consider δD to $\delta^{18}O$ in very dry environments.

The above characterisations led us to propose the following calibration scheme for water vapour isotopes monitoring in Antarctica:

- The humidity dependency showed no particular drift on a 1-year period, so we suggest a humidity-isotope dependency every year using two standards, in the humidity and isotopic range of the site of interest.
- The drift calibration should be performed preferably every 24 to 48 hours, to correct for mid-term drift while keeping enough time for data acquisition. With this calibration scheme, we expect enough resolution on the isotopic signal until humidity values around 10 ppm for δD and 100 ppm for $\delta^{18}O$.

3.2 OF-CEAS performance and comparison with commercial CRDS technique

Signal stability and noise

On short time scales, the OF-CEAS technique permits to reach extreme levels of precision at low water concentrations. We compare in Figure 9 the Allan deviation value at 2 minutes of the commercial CRDS instrument (Picarro) installed at DDU station, and of the two OF-CEAS instruments (AP2E). From 60 to 3000 ppm, the low-humidity OF-CEAS analyser equipped with high reflectivity mirrors shows a noise reduction by a factor of approximately 5 compared to the CRDS and the high-humidity OF-CEAS analyser. This shows the ability for the OF-CEAS technique to capture with a high precision transient events, and demonstrates the potential of the instrument, in particular in the low humidity range where the noise increases exponentially.

https://doi.org/10.5194/egusphere-2024-2149
Preprint. Discussion started: 15 August 2024

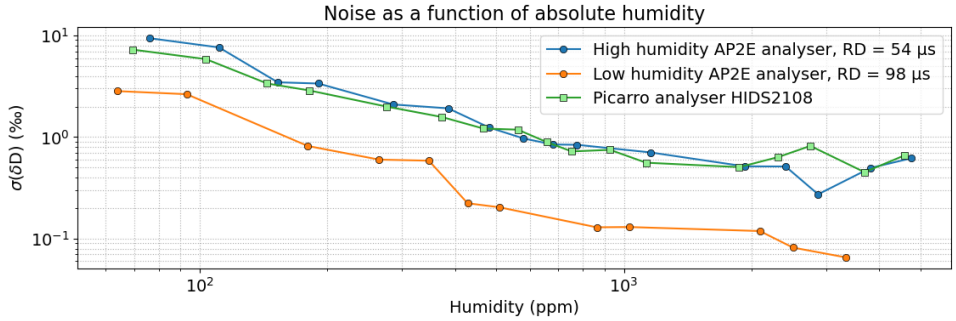

Figure 9 : Noise on δD with an averaging time of 2 min as a function of the humidity for the two OF-CEAS analysers from AP2E and the Picarro analyser currently installed at Dumont d'Urville station. The noise is obtained from short-term Allan deviations at τ = 2 min calculated during each step of the humidity dependency calibration.

On longer timescales, the calibration performed at DDU during 1 year shows no long-term drift on both isotopologues (see Figure 5) neither for the commercial OF-CEAS nor the CRDS instrument, although we observe a higher dispersion on the OF-CEAS dataset (see Table 1).

The particular feature of the OF-CEAS technique is well illustrated on the Allan deviation study presented in section 2.1.1. It shows an optimum stability range of ~ 15 min, followed by a drift period in the hour range and finally a stabilisation of the signal in the day range. We showed in the section above that a calibration every 24 hours – resulting from a compromise between precision and data acquisition time – enabled to keep enough precision to interpret more than 70% of the yearly data on the East Antarctic plateau. However, to get the most out of the analyser precision, a calibration would have to be performed every 10 – 20 minutes, which is not compatible with continuous water isotope measurement.

Unlike the CRDS technique which is based on ring-down time measurements to quantify the water isotopes concentration, the OF-CEAS technique directly measures the transmitted light intensity. This leads for the OF-CEAS to a very fast response and a low instantaneous noise signal, at the expense of a higher sensitivity to interferences. Indeed, the noise measured in OF-CEAS instruments originates from instabilities encountered in the hourly range, as highlighted in the AD calibration, and which we attribute essentially to parasitic interferences. Parasitic interferences in OF-CEAS instruments originate from reflective surfaces situated between the laser and the photodetector, like mirror mounts, polarizers or the metallic gas cell, and can affect the signal. Such interferences are sensitive to temperature variations that can occur especially along the laser to optical cavity path. Two main levers have been identified to optimize the OF-CEAS analyser precision:

- Increase the optical signal stability, by reducing the interferences (efficient optical absorption and thermal regulation, use of low thermal expansion materials), or correct them (use of a reference photodetector, signal post-processing)
- Increase the calibration frequency, by optimising the LHLG settings and reducing the calibration time. For example, using a one standard calibration instead of two, and applying a drying on the humidity generator before sending it to the instrument could lead to a calibration time reduction from 2:35 hours to 40 minutes, which could be performed every 10 hours while maintaining a good time resolution. To further reduce the uncertainties of the calibration and generate identical humidity calibration plateaus over all the year, a temperature regulation of the evaporation chamber of the LHLG is also preferred.

Humidity and isotopic composition dependency

The characterization of the two analysers showed a global linear humidity dependency for humidity levels above 500 ppm. Below 500 ppm, the humidity dependency diverges for different isotope ratios. The low humidity divergence is also observed on commercial CRDS analysers as shown on Figure 6, in particular because both techniques can be affected by a biased fit. Indeed, it has been shown (Weng et al., 2020), (Johnson and Rella, 2017) that broadening or narrowing of the absorption lines

https://doi.org/10.5194/egusphere-2024-2149
Preprint. Discussion started: 15 August 2024

and baseline shift due to changing gas mixture can affect the fitting, thus inducing an error and leading to a humidity and isotope dependency of the measured isotopic composition.

However, to the best of our knowledge, such studies were limited to a minimal humidity value of 500 ppm in most of the calibrations (and 300 ppm for only one calibration, (Weng et al., 2020)). In the case of humidity values below 300 ppm, we think that the presence of residual water in the analyser or in the injection line can also affect the measured signal and create a shift of the isotopic measurement. This is often mentioned as memory effect in the literature (Bailey et al., 2015). A pure drying using the LHLG in the laboratory (with a typical ambient water mixing ratio of 15,000 ppm) without any water injection leads to a residual water of 10 ppm. We can suppose that in this case, the isotopic composition for humidity levels below 100 ppm is affected by the memory effect, i.e. results from a mixing between the injected standard and residual water. This effect is expected to be limited in the field because of a lesser difference between the water mixing ratio inside and outside the instrument. Finally, slight misalignment of the optical components of the instrument after transport (caused by vibrations or thermal expansion), can also impact the transmitted optical spectrum and thus affect the humidity dependency. We insist thus on the importance of calibrating the instrument in the field to correct for those artefacts (Casado et al., 2016).

Interesting features for field operation

In the particular case of field deployment in harsh conditions, there is a great interest for using AP2E OF – CEAS analysers. AP2E spectrometers are made up of optical parts that are mainly assembled mechanically, rather than glued together, making it possible to perform fine optical adjustments in the field or even to remove mirrors for cleaning in case of contamination. The internal architecture of these analysers therefore reduces the risk of breakdowns during the deployment, but requires an expertise to finely tune them. The software offers also the possibility to tune several regulation parameters like for example various temperatures and pressure setpoints and PID parameters to adapt the analyser to the local conditions in the field. Finally, a large number of internal variables are accessible on the instrument, making it possible to quickly diagnose the state of the instrument in the event of a breakdown in the field.

Conclusion

This paper is focused on the characterisation and performance of two water vapour isotope analysers based on new commercial laser spectrometers based on the OF-CEAS technique, particularly adapted for dry regions. The first, “low-humidity” analyser featuring high reflectivity mirrors, has been fully characterised in our laboratory: it shows a low limit of detection and is thus specially adapted to very dry regions such as the East Antarctic plateau. The second, “high-humidity” analyser with slightly lower reflectivity mirrors was installed during the austral summer 2022-2023 in Dumont d’Urville, a coastal station of Antarctica, where humidities are not so low.

The stability of the OF-CEAS analysers has been detailed through long-term AD analysis using the humidity generator, and an unprecedented one-year long calibration measurement has been performed at DDU station and compared to a commercial CRDS analyser, with no visible long-term drift on neither instrument. In addition, the water mixing ratio dependency of the OF-CEAS analyser have been characterized, as well as the accuracy and precision in the low humidity region. We finally estimated the minimum humidity to confidently interpret diurnal cycles at our sites of interest, namely 100 ppm for $\delta^{18}O$ and 10 ppm for δD.

Compared to traditional CRDS analysers used for water isotope monitoring, OF-CEAS analysers equipped with high reflectivity mirrors show an extremely low noise, at the expense of a higher sensitivity to any perturbation of their environment like the temperature. This low noise and fast response open up the possibility to measure transient phenomena, like in-situ measurement of the isotopic composition of individual snowflakes. Moreover, for the particular application of field monitoring in remote areas like Antarctica, these instruments meet the need for an optimizable and adaptable instrument, reducing the

https://doi.org/10.5194/egusphere-2024-2149
Preprint. Discussion started: 15 August 2024

risks of breakdown. The OF-CEAS analyser limitations highlighted in this article concern the instabilities encountered in the hourly range, which we attribute to parasitic interferences. Some solutions to reduce these interferences have been identified, such as managing parasitic reflections with optical absorber, improving the thermal stability inside the instrument or installing a reference photodetector. These new developments are currently implemented, in order to provide the best possible data for the instrumental deployment of the operational units for the AWACA project, planned for the Antarctic season 2024-2025. Beyond Antarctica, other isotopic water vapour monitoring projects, especially in dry conditions or airborne campaigns, could also benefit from the possibilities of these new instruments.

Data availability. The data of this paper is available upon request.

Author contributions. TL optimised the OF-CEAS spectrometers, characterised the instruments, produced all the plots, designed and wrote all sections of the original paper, with inputs from co-authors revising the text. TL and EF installed the instrumentation at DDU during the season 2022-2023. MC and TL wrote the code for the Allan deviation calculation. EF and AL made substantial contributions throughout the paper. DR made substantial contributions on section 2.1 and 3. OJ improved the software to control the calibration instrument (HumGen) and developped an additional software for data processing (HumdepApp). FP, OJ and TL fabricated the calibration instrument. GN made the laboratory calibration plotted in section 2.2 and section 2.3. KJ from AP2E designed the ProCeas® analyser. MM and KJ helped for the optimisation of the OF-CEAS analyser. MF and DR designed and optimised the OF-CEAS prototype. VMD (PI of the ERC Synergy Grant AWACA project) and AL designed the AWACA project.

Competing interests. The authors declare that they have no conflict of interest.

Financial support. This research was supported by the IPEV ADELISE project, and has received funding from the European Research Council (ERC) under the European Union's Horizon 2020 research and innovation program (AWACA grant agreement No 951596).

References

Aemisegger, F., Spiegel, J. K., Pfahl, S., Sodemann, H., Eugster, W., and Wernli, H.: Isotope meteorology of cold front passages: A case study combining observations and modeling, Geophysical Research Letters, 42, 5652–5660, https://doi.org/10.1002/2015GL063988, 2015.

Angert, A., Lee, J.-E., and Yakir, D.: Seasonal variations in the isotopic composition of near-surface water vapour in the eastern Mediterranean, Tellus B: Chemical and Physical Meteorology, 60, 674–684, https://doi.org/10.1111/j.1600-0889.2008.00357.x, 2008.

Bailey, A., Noone, D., Berkelhammer, M., Steen-Larsen, H. C., and Sato, P.: The stability and calibration of water vapor isotope ratio measurements during long-term deployments, Atmospheric Measurement Techniques, 8, 4521–4538, https://doi.org/10.5194/amt-8-4521-2015, 2015.

Benetti, M., Aloisi, G., Reverdin, G., Risi, C., and Sèze, G.: Importance of boundary layer mixing for the isotopic composition of surface vapor over the subtropical North Atlantic Ocean, Journal of Geophysical Research: Atmospheres, 120, 2190–2209, https://doi.org/10.1002/2014JD021947, 2015.

Benetti, M., Lacour, J.-L., Sveinbjörnsdóttir, A. E., Aloisi, G., Reverdin, G., Risi, C., Peters, A. J., and Steen-Larsen, H. C.: A Framework to Study Mixing Processes in the Marine Boundary Layer Using Water Vapor Isotope Measurements, Geophysical Research Letters, 45, 2524–2532, https://doi.org/10.1002/2018GL077167, 2018.

Bhattacharya, S. K., Sarkar, A., and Liang, M.-C.: Vapor Isotope Probing of Typhoons Invading the Taiwan Region in 2016, Journal of Geophysical Research: Atmospheres, 127, e2022JD036578, https://doi.org/10.1029/2022JD036578, 2022.

https://doi.org/10.5194/egusphere-2024-2149
Preprint. Discussion started: 15 August 2024

Bonne, J.-L., Masson-Delmotte, V., Cattani, O., Delmotte, M., Risi, C., Sodemann, H., and Steen-Larsen, H. C.: The isotopic composition of water vapour and precipitation in Ivittuut, southern Greenland, Atmospheric Chemistry and Physics, 14, 4419–4439, https://doi.org/10.5194/acp-14-4419-2014, 2014.

Bonne, J.-L., Meyer, H., Behrens, M., Boike, J., Kipfstuhl, S., Rabe, B., Schmidt, T., Schönicke, L., Steen-Larsen, H. C., and Werner, M.: Moisture origin as a driver of temporal variabilities of the water vapour isotopic composition in the Lena River Delta, Siberia, Atmos. Chem. Phys., 20, 10493–10511, https://doi.org/10.5194/acp-20-10493-2020, 2020.

Bréant, C., Leroy Dos Santos, C., Agosta, C., Casado, M., Fourré, E., Goursaud, S., Masson-Delmotte, V., Favier, V., Cattani, O., Prié, F., Golly, B., Orsi, A., Martinerie, P., and Landais, A.: Coastal water vapor isotopic composition driven by katabatic wind variability in summer at Dumont d'Urville, coastal East Antarctica, Earth and Planetary Science Letters, 514, 37–47, https://doi.org/10.1016/j.epsl.2019.03.004, 2019.

Casado, M., Landais, A., Masson-Delmotte, V., Genthon, C., Kerstel, E., Kassi, S., Arnaud, L., Picard, G., Prie, F., Cattani, O., Steen-Larsen, H.-C., Vignon, E., and Cermak, P.: Continuous measurements of isotopic composition of water vapour on the EastAntarctic Plateau, Atmos. Chem. Phys., 16, 8521–8538, https://doi.org/10.5194/acp-16-8521-2016, 2016.

Dietrich, L. J., Steen-Larsen, H. C., Wahl, S., Jones, T. R., Town, M. S., and Werner, M.: Snow-Atmosphere Humidity Exchange at the Ice Sheet Surface Alters Annual Mean Climate Signals in Ice Core Records, Geophysical Research Letters, 50, e2023GL104249, https://doi.org/10.1029/2023GL104249, 2023.

Galewsky, J., Steen-Larsen, H. C., Field, R. D., Worden, J., Risi, C., and Schneider, M.: Stable isotopes in atmospheric water vapor and applications to the hydrologic cycle, Reviews of Geophysics, 54, 809–865, https://doi.org/10.1002/2015RG000512, 2016.

Gupta, P., Noone, D., Galewsky, J., Sweeney, C., and Vaughn, B. H.: Demonstration of high-precision continuous measurements of water vapor isotopologues in laboratory and remote field deployments using wavelength-scanned cavity ring-down spectroscopy (WS-CRDS) technology, Rapid Commun Mass Spectrom, 23, 2534–2542, https://doi.org/10.1002/rcm.4100, 2009.

Henze, D., Noone, D., and Toohey, D.: Aircraft measurements of water vapor heavy isotope ratios in the marine boundary layer and lower troposphere during ORACLES, Earth Syst. Sci. Data, 14, 1811–1829, https://doi.org/10.5194/essd-14-1811-2022, 2022.

Hughes, A. G., Wahl, S., Jones, T. R., Zuhr, A., Hörhold, M., White, J. W. C., and Steen-Larsen, H. C.: The role of sublimation as a driver of climate signals in the water isotope content of surface snow: laboratory and field experimental results, The Cryosphere, 15, 4949–4974, https://doi.org/10.5194/tc-15-4949-2021, 2021.

Johnson, J. E. and Rella, C. W.: Effects of variation in background mixing ratios of N2, O2, and Ar on the measurement of d18O–H2O and d2H–H2O values by cavity ring-down spectroscopy, Atmos. Meas. Tech., 10, 3073–3091, https://doi.org/10.5194/amt-10-3073-2017, 2017.

Kerstel, E.: Modeling the dynamic behavior of a droplet evaporation device for the delivery of isotopically calibrated low-humidity water vapor, Atmos. Meas. Tech., 14, 4657–4667, https://doi.org/10.5194/amt-14-4657-2021, 2021.

Kopec, B. G., Lauder, A. M., Posmentier, E. S., and Feng, X.: The diel cycle of water vapor in west Greenland, Journal of Geophysical Research: Atmospheres, 119, 9386–9399, https://doi.org/10.1002/2014JD021859, 2014.

Landais, A., Agosta, C., Vimeux, F., Magand, O., Solis, C., Cauquoin, A., Dutrievoz, N., Risi, C., Leroy-Dos Santos, C., Fourré, E., Cattani, O., Jossoud, O., Minster, B., Prié, F., Casado, M., Dommergue, A., Bertrand, Y., and Werner, M.: Abrupt excursions in water vapor isotopic variability at the Pointe Benedicte observatory on Amsterdam Island, Atmospheric Chemistry and Physics, 24, 4611–4634, https://doi.org/10.5194/acp-24-4611-2024, 2024.

Landsberg, J., Romanini, D., and Kerstel, E.: Very high finesse optical-feedback cavity-enhanced absorption spectrometer for low concentration water vapor isotope analyses, Opt. Lett., 39, 1795, https://doi.org/10.1364/OL.39.001795, 2014.

Leroy-Dos Santos, C., Casado, M., Prié, F., Jossoud, O., Kerstel, E., Farradèche, M., Kassi, S., Fourré, E., and Landais, A.: A dedicated robust instrument for water vapor generation at low humidity for use with a laser water isotope analyzer in cold and dry polar regions, Atmos. Meas. Tech., 14, 2907–2918, https://doi.org/10.5194/amt-14-2907-2021, 2021.

Leroy-Dos Santos, C., Fourré, E., Agosta, C., Casado, M., Cauquoin, A., Werner, M., Minster, B., Prié, F., Jossoud, O., Petit, L., and Landais, A.: From atmospheric water isotopes measurement to firn core interpretation in Adelie Land: A case study for isotope-enabled atmospheric models in Antarctica, Snow/Atmospheric Interactions, https://doi.org/10.5194/egusphere-2023-447, 2023.

https://doi.org/10.5194/egusphere-2024-2149
Preprint. Discussion started: 15 August 2024

Merlivat, L. and Nief, G.: Fractionnement isotopique lors des changements d'état solide-vapeur et liquide-vapeur de l'eau à des températures inférieures à 0°C, Tellus, 19, 122–127, https://doi.org/10.1111/j.2153-3490.1967.tb01465.x, 1967.

Ritter, F., Steen-Larsen, H. C., Werner, M., Masson-Delmotte, V., Orsi, A., Behrens, M., Birnbaum, G., Freitag, J., Risi, C., and Kipfstuhl, S.: Isotopic exchange on the diurnal scale between near-surface snow and lower atmospheric water vapor at Kohnen station, East Antarctica, The Cryosphere, 10, 1647–1663, https://doi.org/10.5194/tc-10-1647-2016, 2016.

Romanini, D., Ventrillard, I., Méjean, G., Morville, J., and Kerstel, E.: Introduction to Cavity Enhanced Absorption Spectroscopy, in: Cavity-Enhanced Spectroscopy and Sensing, vol. 179, edited by: Gagliardi, G. and Loock, H.-P., Springer Berlin Heidelberg, Berlin, Heidelberg, 1–60, https://doi.org/10.1007/978-3-642-40003-2_1, 2014.

Thurnherr, I., Kozachek, A., Graf, P., Weng, Y., Bolshiyanov, D., Landwehr, S., Pfahl, S., Schmale, J., Sodemann, H., Steen-Larsen, H. C., Toffoli, A., Wernli, H., and Aemisegger, F.: Meridional and vertical variations of the water vapour isotopic composition in the marine boundary layer over the Atlantic and Southern Ocean, Atmospheric Chemistry and Physics, 20, 5811–5835, https://doi.org/10.5194/acp-20-5811-2020, 2020.

Tremoy, G., Vimeux, F., Soumana, S., Souley, I., Risi, C., Favreau, G., and Oï, M.: Clustering mesoscale convective systems with laser-based water vapor δ18O monitoring in Niamey (Niger), Journal of Geophysical Research: Atmospheres, 119, 5079–5103, https://doi.org/10.1002/2013JD020968, 2014.

Wahl, S., Steen-Larsen, H. C., Reuder, J., and Hörhold, M.: Quantifying the Stable Water Isotopologue Exchange Between the Snow Surface and Lower Atmosphere by Direct Flux Measurements, Journal of Geophysical Research: Atmospheres, 126, e2020JD034400, https://doi.org/10.1029/2020JD034400, 2021.

Weng, Y., Touzeau, A., and Sodemann, H.: Correcting the impact of the isotope composition on the mixing ratio dependency of water vapour isotope measurements with cavity ring-down spectrometers, Atmos. Meas. Tech., 13, 3167–3190, https://doi.org/10.5194/amt-13-3167-2020, 2020.